Comparing PNe with the nebulae surrounding massive stars in the LMC

Warren Reid[1,2]

[1]Macquarie University, Sydney, Australia;
[2]Macquarie Centre for Astronomy, Astrophysics and Astrophotonics

Although the physics governing the atmospheres and associated nebula emission in hot emission line stars is markedly different from the processes contributing to the formation of a PN, these objects can mimic one other and are often confused. The extended atmospheres common to both mean that subtracted Hα/red and other optical images may not be sufficient to provide an accurate identification. Our analysis of 579 hot emission-line stars and 715 PNe within the LMC - the largest set of spectroscopically confirmed objects in any eternal galaxy - has provided us with an extensive database of spectral classifications, rotational and radial velocities, object variability and emission line profiles. This greatly assists in the differentiation of these two populations.

Introduction

The Large Magellanic Cloud (LMC) is a unique laboratory in which to study the characteristics of massive and luminous emission-line stars. At a known distance of 50 kpc (see Reid & Parker 2010 and references therein), modest inclination angle to the line of sight (21°) and with relatively low interstellar extinction (Rv= 3.41 ±0.06; Gordon et al. 2003), apparent brightness is a good indicator of absolute luminosity to within a few tenths of a magnitude. This simplifies the identification, analysis and comparison of emission-line stars and PNe in the LMC. The most important observational feature of the emission-line stellar group is the presence of the Hα line. The presence of this emission line has been widely used as an identifier in many previous searches for emission-line stars in the LMC (eg. Henize 1956; Bohannan & Epps 1974; Grebel & Chu 2000; Keller et al. 2000; Olsen et al. 2001; Reid & Parker 2012). It has also been used as a initial identifier for PNe (Reid & Parker 2006a,b).

Our spectroscopic follow-up has revealed 579 hot emission-line stars with spectral classes B-F out of a total sample of 1,062 emission-line stars of all spectral types uncovered. Only 111 of these were previously known whereas 469 are newly discovered (Reid & Parker 2012).

Be stars are known to be variables which undergo active and quiescent stages (Bjorkman et al. 2002). With known variability, the OGLE II database has recently become the main tool used to uncover emission-line star candidates (Sabogal et al. 2005). A single epoch survey could miss many of these stars if they were undergoing a quiescent stage. Our Hα survey, utilising 12 Hα exposures taken over a three year period has largely alleviated such problems and revealed a large number of emission-line stars in the survey region to a magnitude of R_{equiv} 22 for Hα.
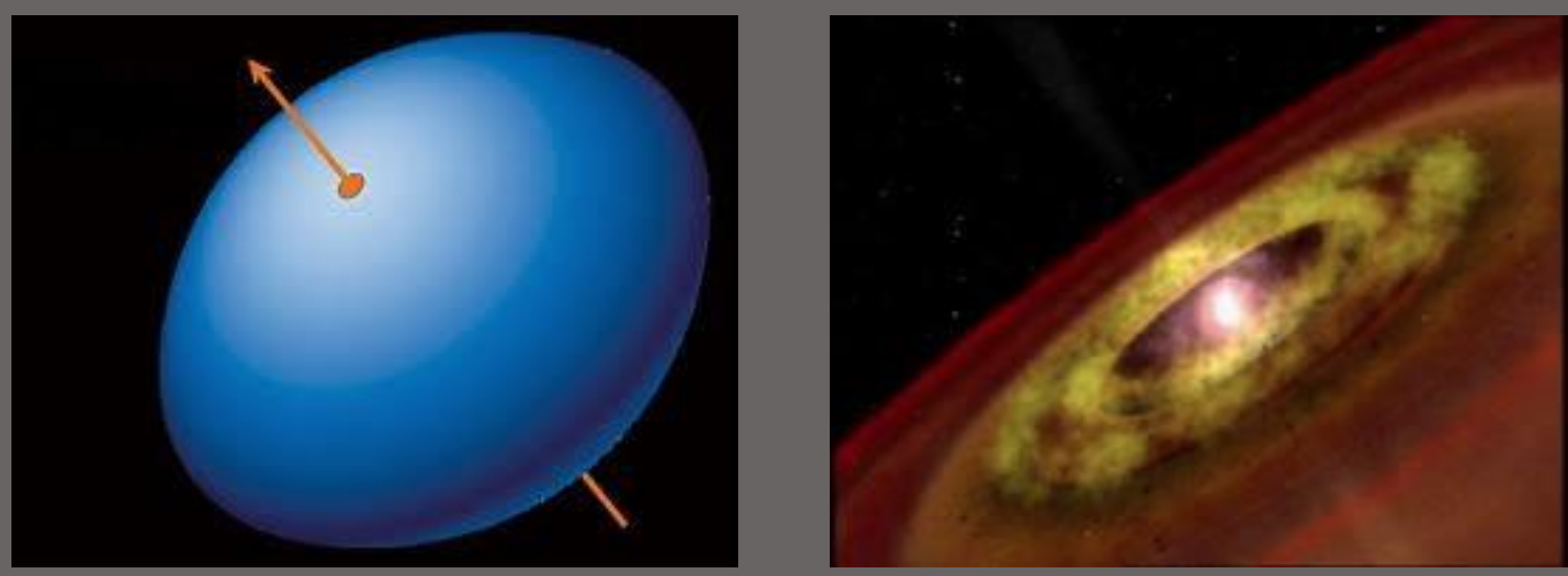

Figure 1. Various models have been proposed to explain how gaseous disks form around Be stars. These include, wind-compressed models, the magnetospheric accretion model, outbursts, shell phases and models based on rotational velocities resulting in a strange form of variability. Winds may also drive non-radial pulsations, producing subtle magnitude variations and changing the shape of absorption lines.
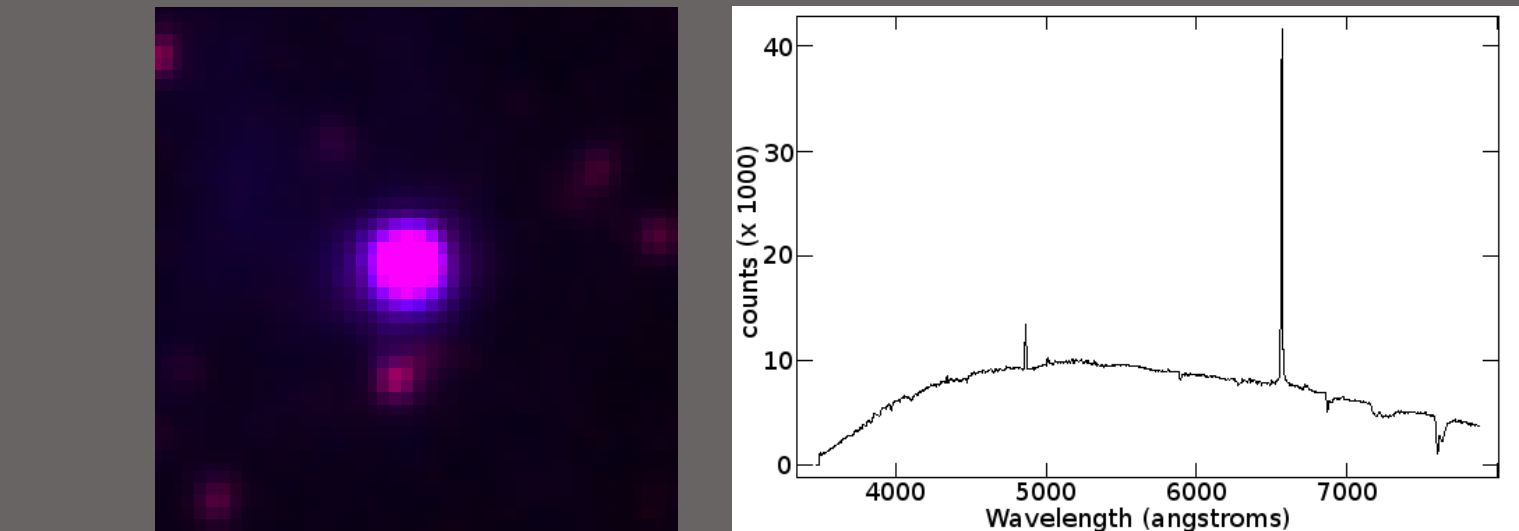

Figure 2. Hα (blue) /SR (red) 30 × 30 arcsec image and 2dF low resolution spectrum of RPs255, also known as BE474 (Bohannan & Epps, 1974) and L333 (Lindsay, 1963). M (Hα)=16.37. North is upwards.
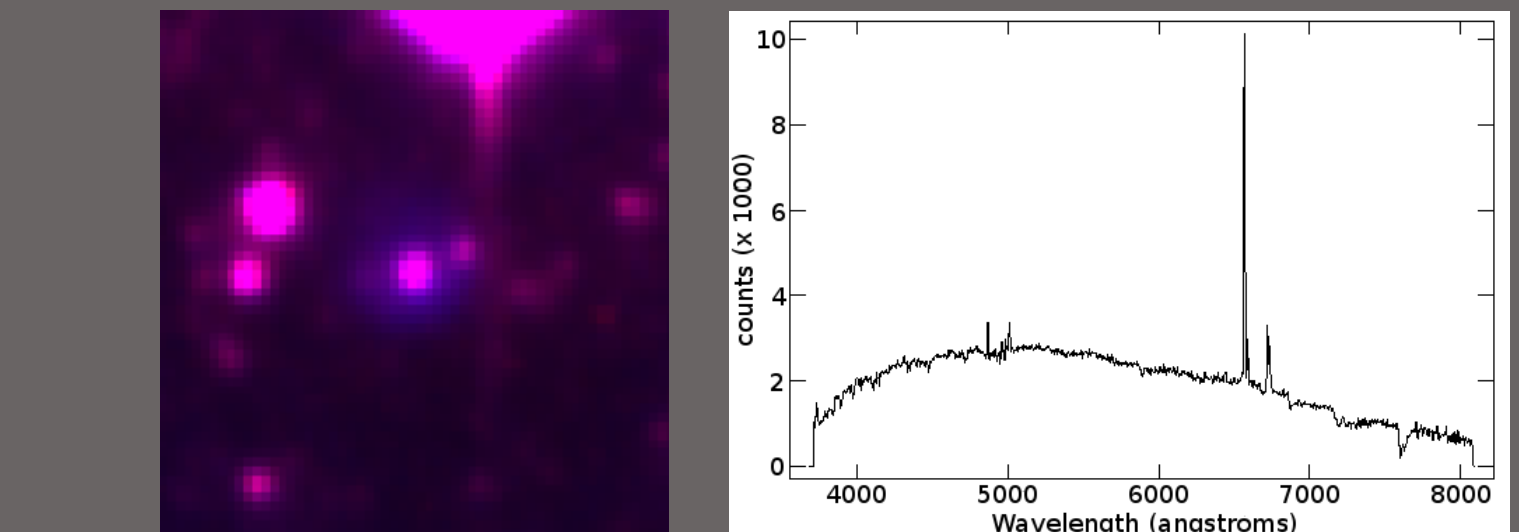

Figure 3. Same as above for newly discovered emission-line star RPs256. M (Hα)=19.34. The presence of forbidden lines indicates a B[e] star.

Spectral classification

The classification of emission-line stars is complex and often problematic due to their variability and atmospheric activity. The strength and profile of the Balmer lines in emission only lend moderate assistance to classification, although the equivalent width of Hγ can be a good indicator of spectral type and luminosity in main sequence blue (Underhill & Doazan 1982).

To assign a spectral classification, it is necessary to measure the strength and width of specific absorption lines which depict stellar temperatures and surface gravities, independent of any associated emission characteristics. As templates for this process we used standard stellar spectra supplemented by 10 emission-line stars from our LMC sample with known spectral classifications.

In order to produce the most accurate match through cross-correlation, all emission lines (including any residual telluric sky lines which can effect the cross-correlation) were removed. The continuum was then removed using the IRAF CONTINUUM task in order to use the absorption lines alone. This negated the influence of the continuum where it was either stronger or weaker than the best matching spectrum in the continuum subtracted templates. Apodization within XCSAO uses a cosine bell to attenuate data on the ends of the spectrum, reducing high wave number fourier components that would be produced by abrupt cutoffs at the ends of the spectra, effectively smoothing out the continuum across the full length of the spectrum. Examples below in figure 4 show only the blue end of the optical spectrum which contains the main diagnostic lines for spectral classification.
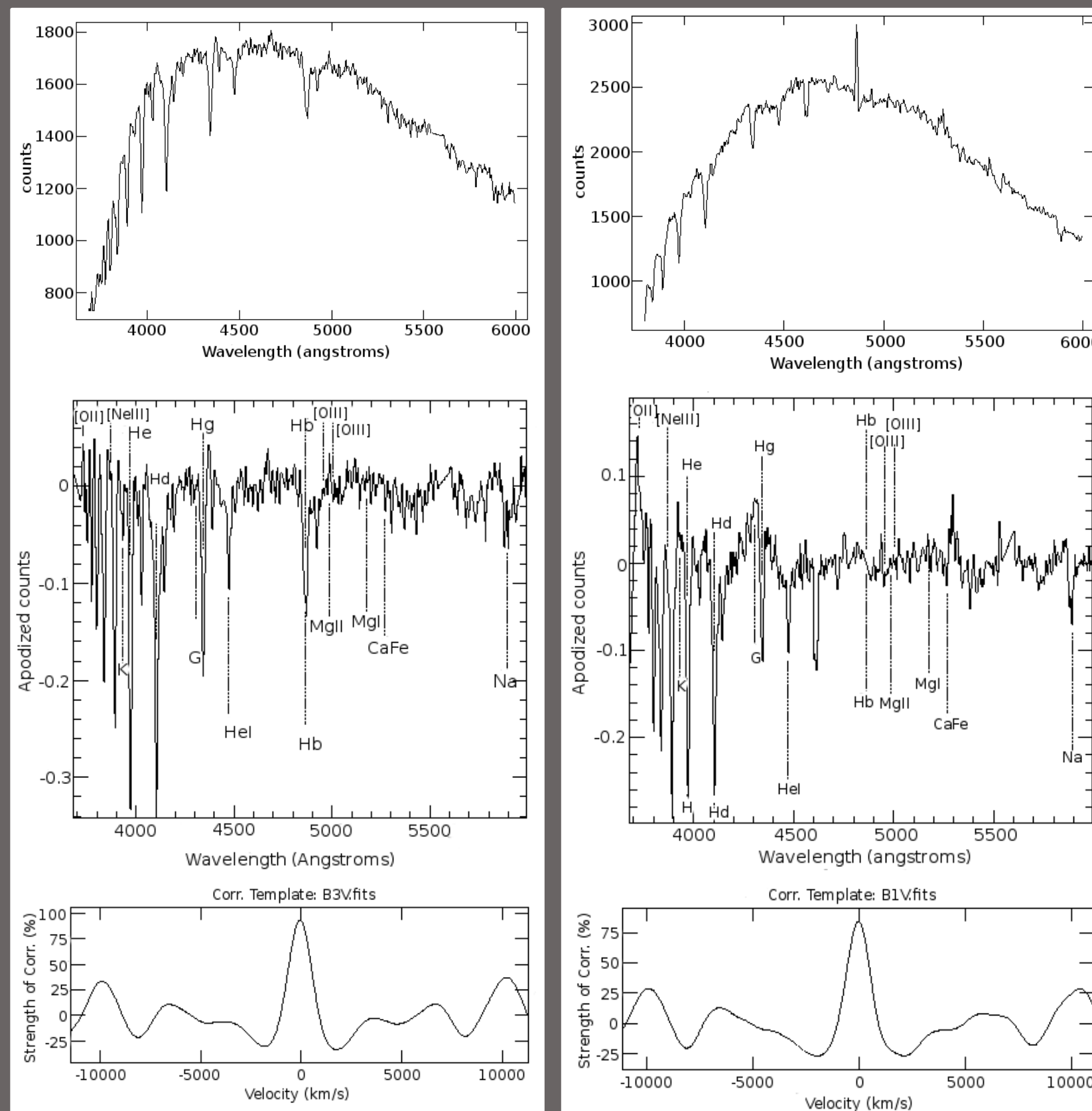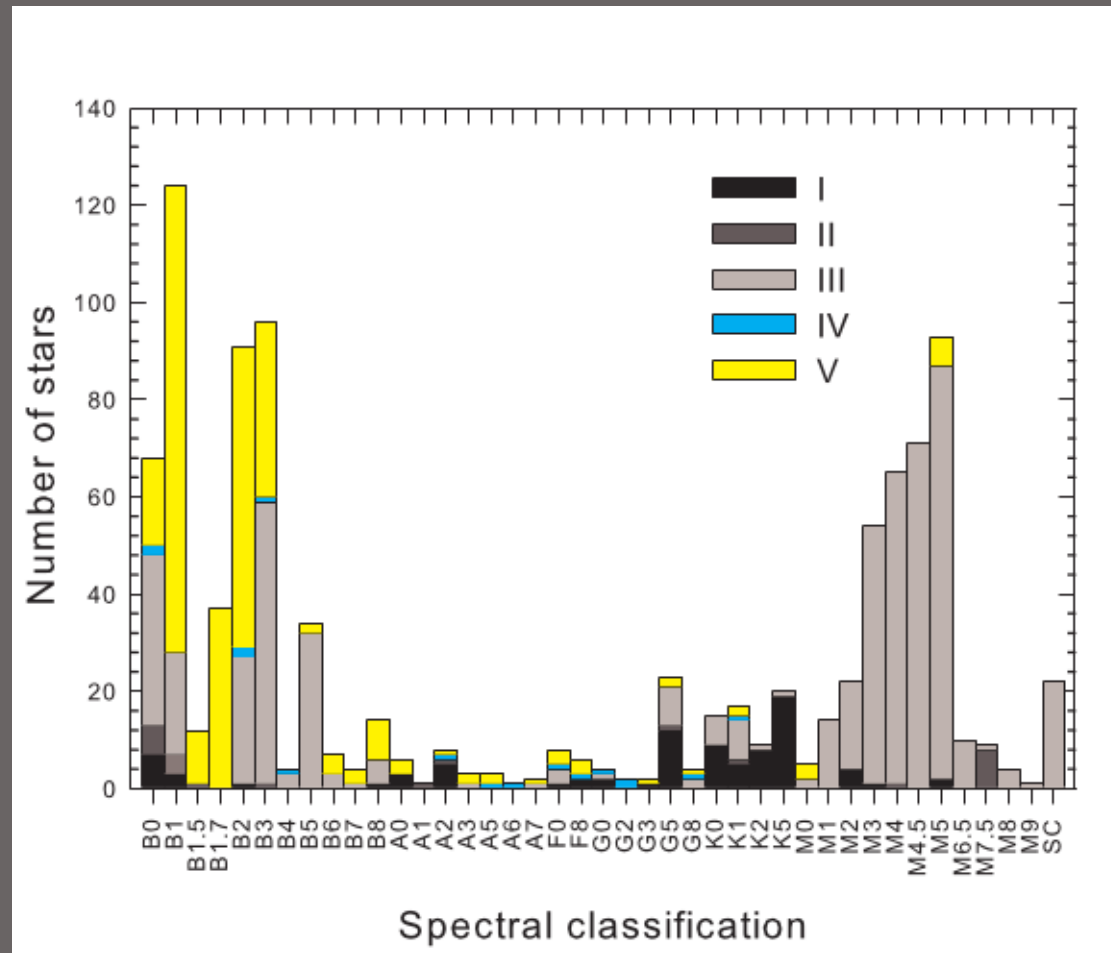

Figure 4. The top images show the blue end of the RPs1326 and RP1262 optical spectrum prior to the removal of emission-lines and continuum. The centre frames show the apodized and continuum subtracted spectra, created within XCSAO and used in cross-correlation to match the best fitting template. The gaussian curve in the lower frames shows the strength of the resulting correlation, once the optimum fit is found.

Figure 5. (spectral classification histogram)
Spectral classification

In Figure 5 we show the results of spectral classification for >1000 emission line stars including late-type stars. Due to their cooler temperature, these stars have an SED that peaks towards the red end of the spectrum. They often exhibit strong excess Hα emission originating from the chromosphere which strengthens with increasing spectral type or decreasing luminosity. The number of stars in each spectral classification is subdivided into luminosity class of the star according to the Morgan-Keenan system. Class SC may be divided into 4 × SC4/9 stars, 1 × S4/2, 1 S4/6 and 16 carbon stars, 13 of which are C6.

Emission lines in Be and B[e] stars compared to PNe

From our 468 newly discovered hot B0-B9 emssion-line stars, we identified 107 B[e] stars that exhibit forbidden emission-lines with [OIII] λ5007/Hβ ratios that can mimic PNe. The most common forbidden emission-lines found in the B[e] stars were [FeII] λ4244,4287,4415,5273,7155, [OI] λ6300,6363, [NII] λ5755,6548,6584, [SII] λ4068,6717,6730, [OII] λ7320, 7330, and [OIII] λ4959,5007, the most frequent being [FeII] and [OI]. The ionisation potential of the last two, less than 25eV, is lower than the ion energies found in planetary nebulae.

We also identified early B-type stars with anomalies (weak or strong) in carbon, nitrogen and usually oxygen. These were first labeled CNO stars by Jaschek & Jaschek (1967). The stars with anomalies in their heavier elements are called Bp stars, where 'p' designates 'peculiar'. We have identified 5 Bp candidates. They are particularly enhanced in Si λ4200, Mn II, Cr II, Eu II and Sr II.

Emission-line profiles

Unlike those of PNe (Figures 6 & 7), the emission line profiles of Be and B[e] stars (Figures 8-11) can represent a combination of instrumental broadening, small absorption features which are often broadened by rotation originating from the photosphere of the star and the emission-line profile produced by the star's circumstellar envelope. Emission and absorption lines may both include kinematic and non-kinematic broadening from effects such as radiative transfer and Thomson scattering which affect the envelope (eg. Hanuschik, 1989). Absorption lines are generally less affected leaving emission lines to provide important information about the rotation and physical conditions affecting the star and it's circumstellar envelope.

The Balmer emission lines in Be and B[e] stars demonstrate the most diverse range of profiles. Profile variations are believed to be dependent on the observer's angle of inclination to the star's pole. According to the model of Struve (1931), shell profiles occur where the star is viewed equatorially (i = 90 deg), double peaked profiles occur at mid-inclination angles and singly peaked profiles occur by viewing towards the pole (I = 0 deg). The measurement of accurate inclination angles, however, is complicated by other influences on the profile such as temperature, density and rotational velocity.
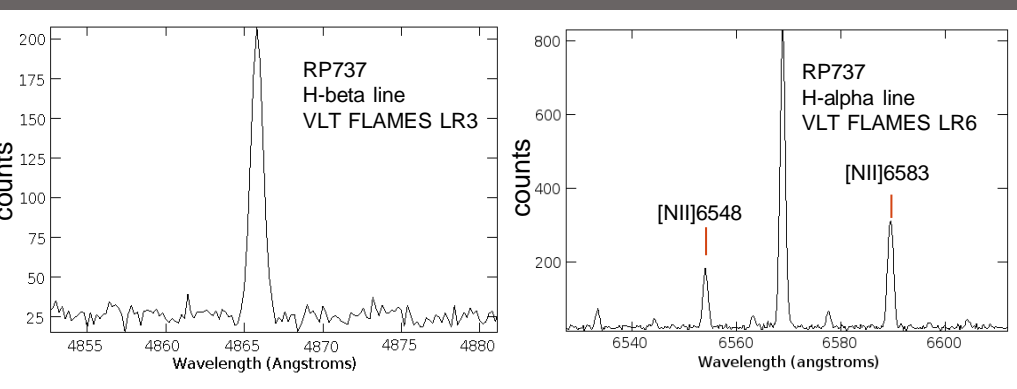

Figure 6. An PN emission line profile for RP737 featuring Hβ (left image FLAMES LR3 grating) and Hα at the centre in the right image (FLAMES LR6 grating).
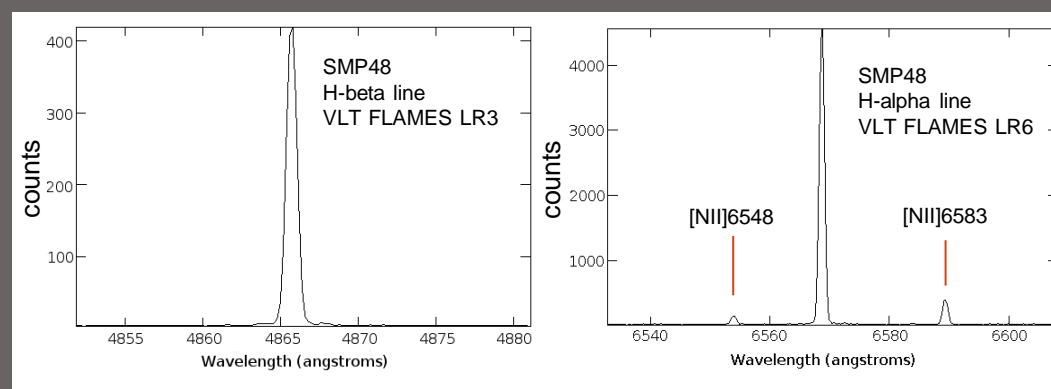

Figure 6. An PN emission line profile for SMP48 featuring Hβ (left image FLAMES LR3 grating) and Hα at the centre in the right image (FLAMES LR6 grating).
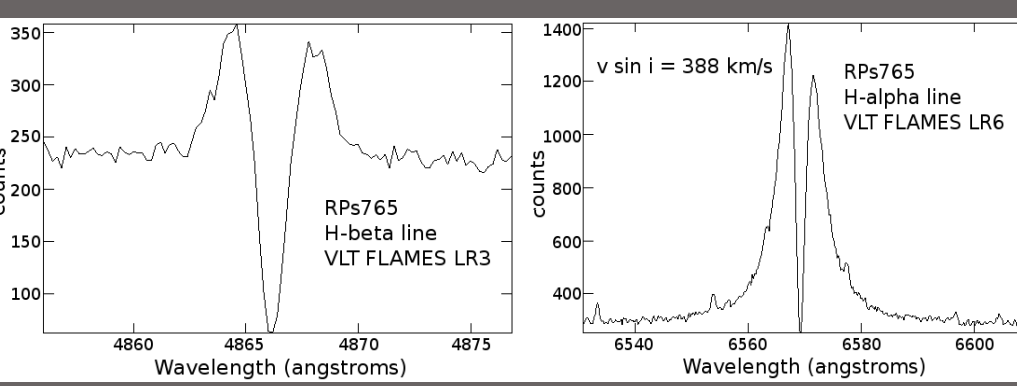

Figure 8. An example of Balmer line splitting, typical of a 'shell star' or more correctly, a star going through a shell phase, where the central absorption on the Hβ line extends below the stellar continuum. The example shown is RPs765 with Hβ left (FLAMES LR3 grating) and Hα right (FLAMES LR6 grating).
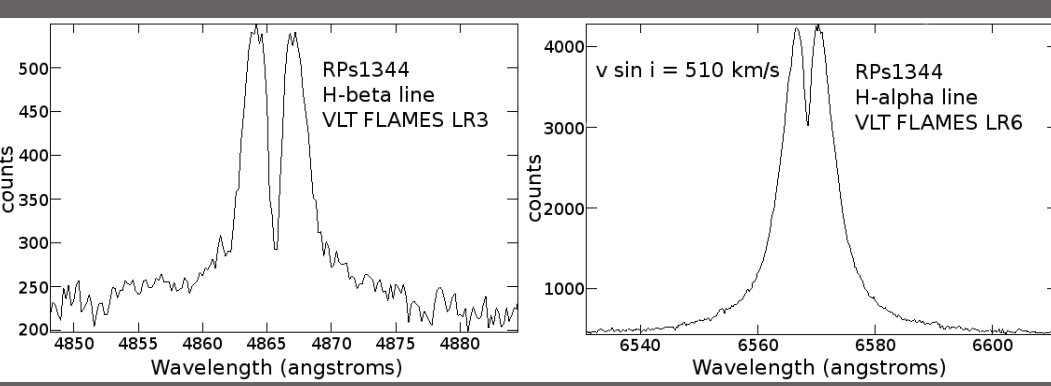

Figure 9. An example of Balmer line splitting in the high velocity circumstellar region of RPs1344 with Hβ left (FLAMES LR3 grating) and Hα right (FLAMES LR6 grating). The narrow profile of the shell absorption line indicates its origin closer to the outer, slowly rotating parts of the shell.
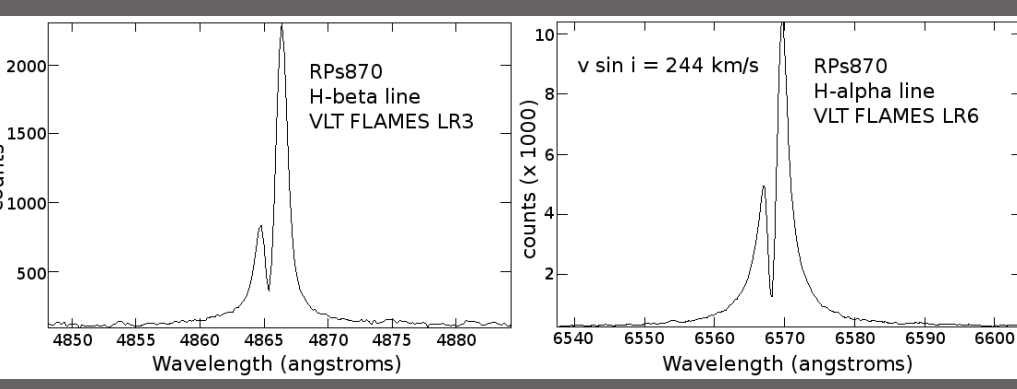

Figure 10. RPs870 is an example of Balmer line splitting which appears to the left of centre with Hβ left (FLAMES LR3 grating) and Hα right (FLAMES LR6 grating). The peak R>V affects both hydrogen emission lines and arises from one-armed density waves in the circumstellar disk.
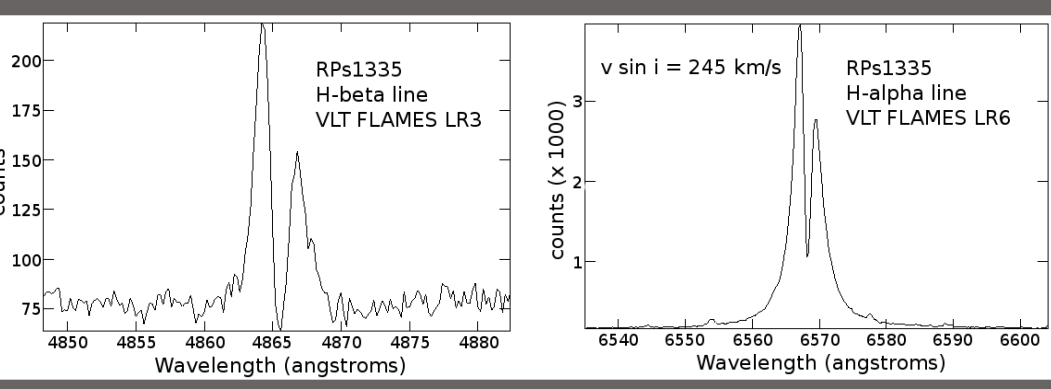

Figure 11. RPs1335 is an example of Balmer line splitting which appears to the right of centre with Hβ left (FLAMES LR3 grating) and Hα right (FLAMES LR6 grating). In this case V>R.

Rotational velocities of Be stars compared to the central stars of PNe

Classical Be stars undergo rapid rotation and possess geometrically thin, circular gaseous disks resulting in hydrogen Balmer emission. Typical rotation compared to critical velocity (v_{eq}/v_{crit}) has been estimated at 70%-80% (Porter 1996). Due to fast rotation it is expected that the star is flattened, causing a variation in temperature and density from pole to equator. This is expected to result in a gravitational darkening of the stellar disk. To derive the projected rotational velocity (v sin i) we used the correlation found by Dachs et al. (1986, Equation (7)) with improvements made by Hanuschik (1989). Their three parameter correlation between FWHM (H), v sin i and equivalent width (EW) lead to the relation:

$$v \sin i = [(FWHM(H\alpha) + 10^{0.08 \log EW + 0.14}) / 1.23] − 70$$

The relationship of FWHM to v sin i is shown in Figure 10. A histogram giving the frequency of v sin i for a selection of LMC PNe versus hot emission-line stars in the LMC and the Galaxy is shown in Figure 11.
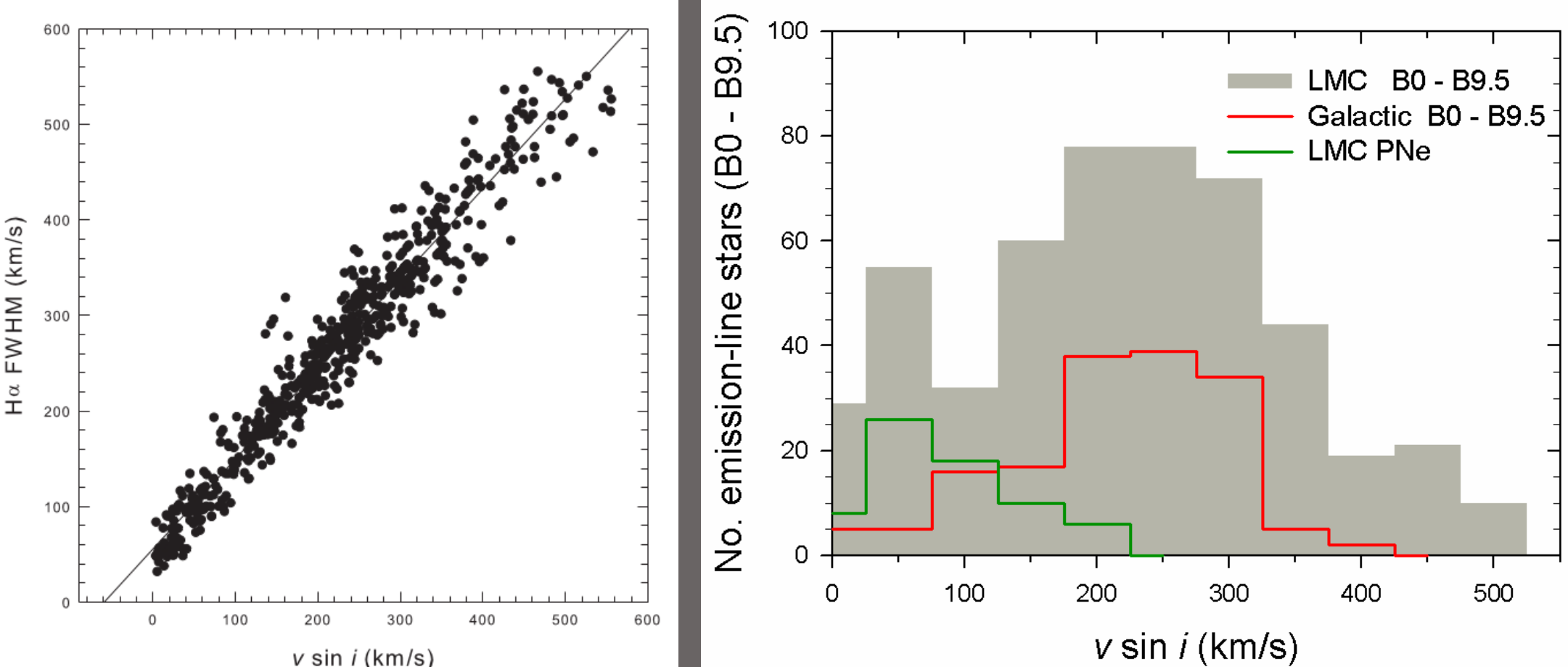

Figure 10. The relation between FWHM measured on the Hα line and the rotational velocity (v sin i) using equation (above) for all emission-line stars in our sample. The variations away from the line of equality are mainly due to the equivalent width, used to determine v sin i.

Figure 11. The distribution of rotational velocities (v sin i) for all Be stars (B0 - B9.5) in our LMC sample compared to the distribution for Galactic Be stars (B0 - B9.5) and 68 PNe from the LMC. Calculations for emission line stars use helium absorption lines whereas those for PNe central stars use [NII] lines found at the lowest and closest zone to the central star.

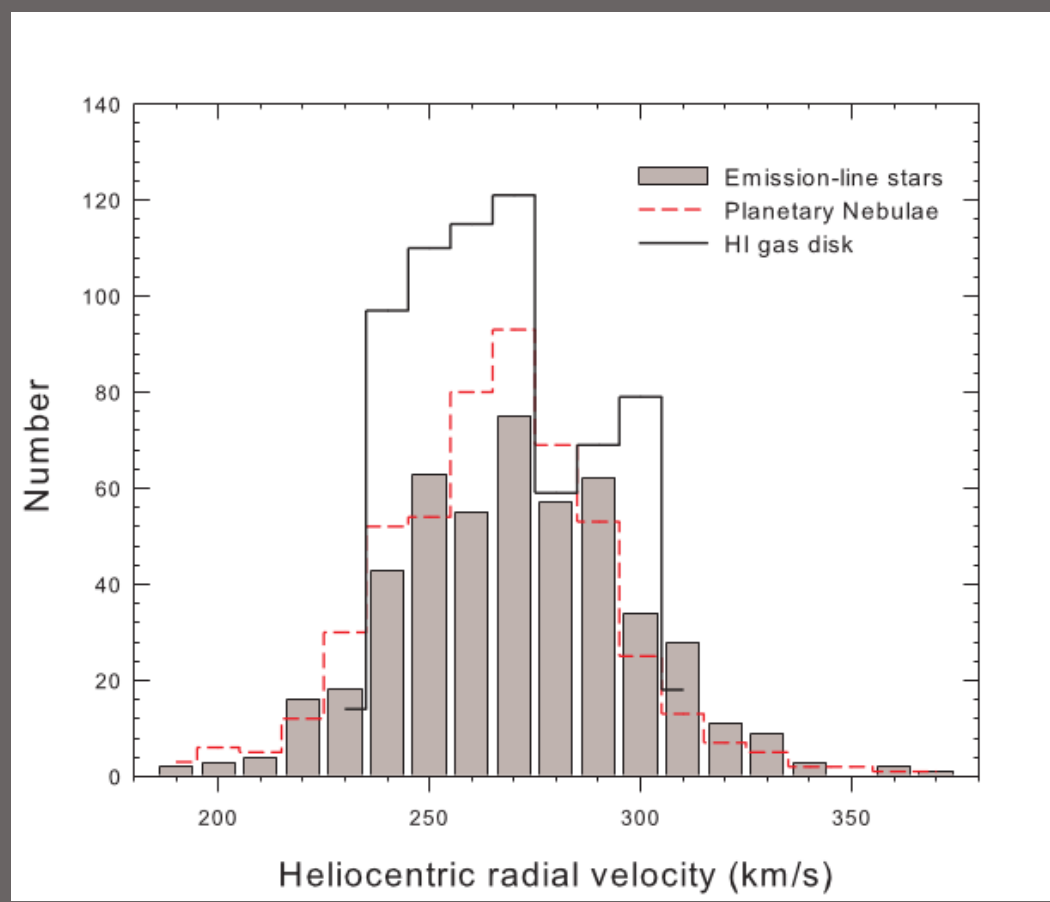## Radial velocities for LMC PNe and emission line stars

Figure 12. (left) shows the distribution of LMC emission-line star velocities by number and compared to the distribution for PNe and the HI gas disk. All sources have been placed into 10km s^{-1} heliocentric radial velocity bins. The emission-line stars lie within the range previously found for LMC PNe and HII regions, which is about 40km s^{-1} wider at each end than the HI distribution. All three distributions share a mean peak number of sources at 270kms[-1]. The HI has a sudden trough after the peak (280km s^{-1}) due to a warp which lies north of the main bar along the line of nodes (see Reid & Parker 2006b).
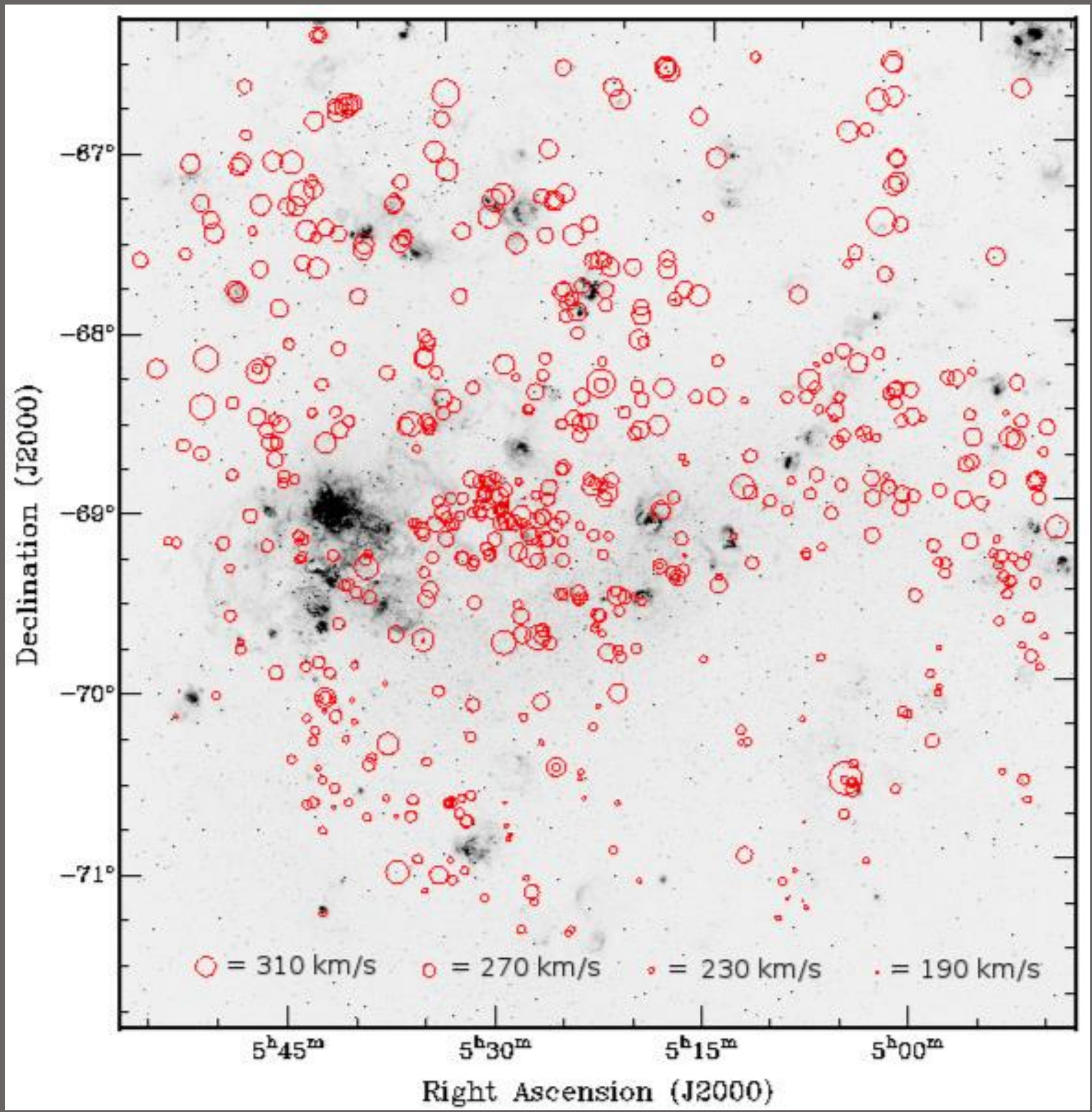

Figure 13. An Hα map of the central 25deg² region of the LMC showing the distribution of hot emission-line stars as open red circles, the size of which indicates the measured heliocentric radial velocity. The larger the diameter, the higher the velocity. The circle sizes are based on a linear scale and magnified 10x in order to emphasis similarities and contrast the variations within selected areas. Like the HI gas disk, the PNe and HII populations have a noticeable gradient from high velocities NE of the main bar to low velocities SW of the main bar. The average velocity of 270km s^{-1} for emission-line stars is also common to all three populations on the main bar.
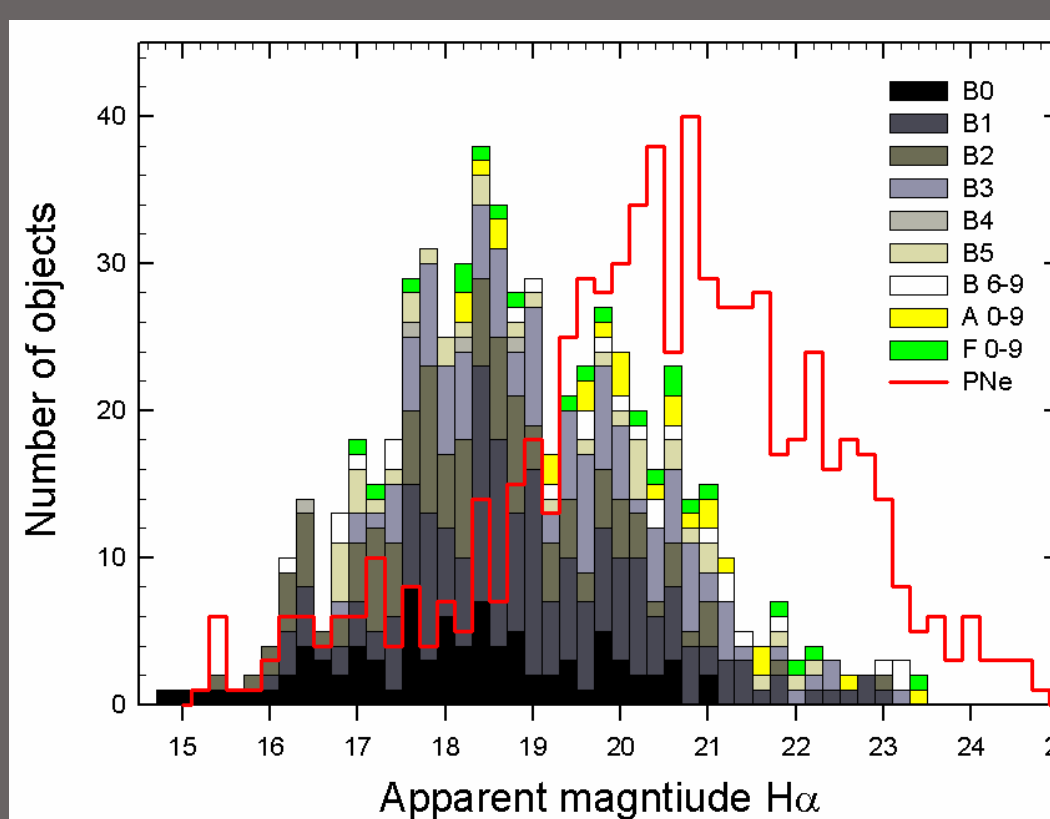
Photometry

Figure 14. The Hα luminosity function for PNe (red line) and emission line stars across the whole LMC. The luminosity bins are 0.2 magnitudes and spectral classifications are indicated in the legend.
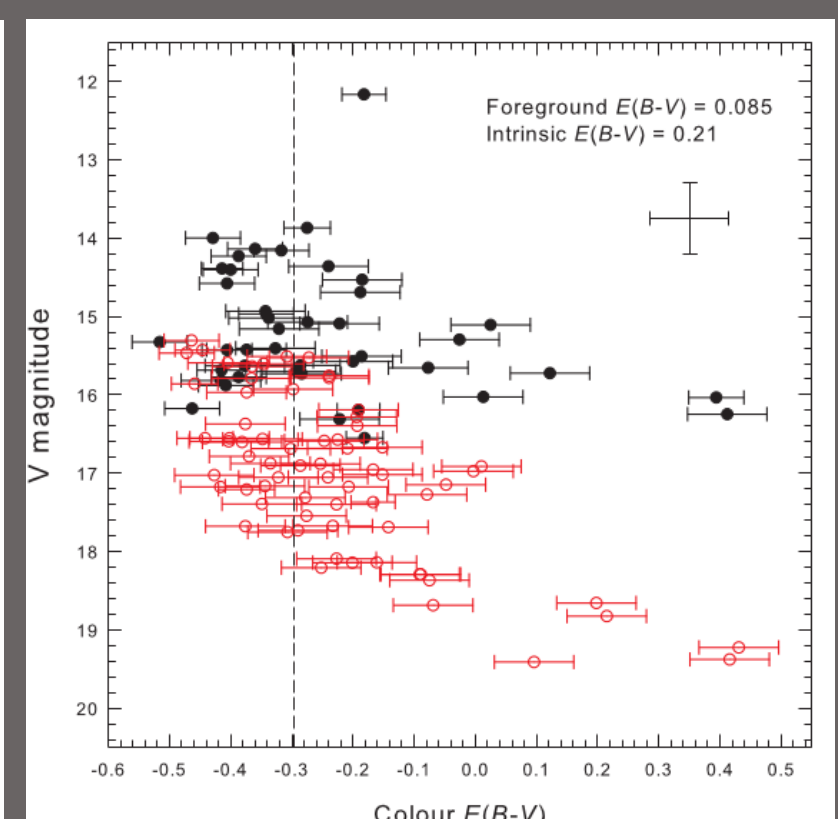
Figure 15. The V versus E(B-V) colour-magnitude diagram from OGLE-II photometry for 117 variable hot emission-line stars found on the LMC main bar. Main sequence stars are assigned red open circles while giant stars are represented by filled black circles. We assume a combined foreground and intrinsic reddening of E(B-V) = 0.295. Error bars are based on a combination of B and V published error estimates for B stars on or very close to the main bar. Maximum errors on both scales are shown. The observed position of (B-V) = 0 is shown by the broken vertical line.
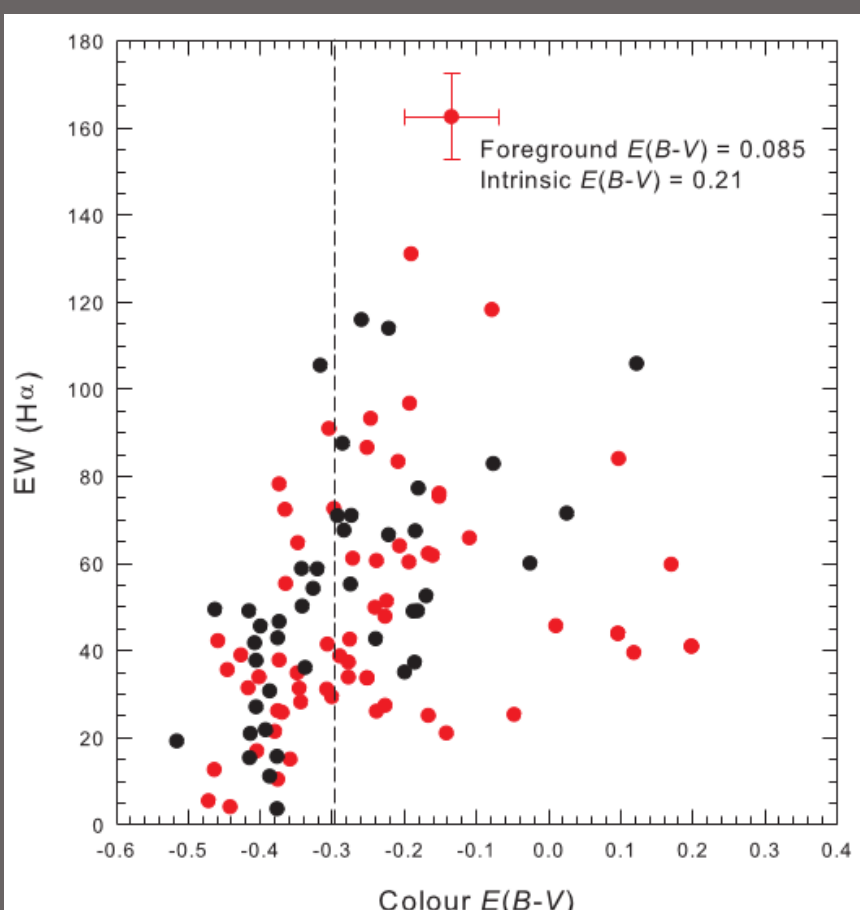

Figure 16. The equivalent width (Hα) versus E(B-V) colour diagram using our measured Hα magnitudes and averaged OGLE-II photometry for 100 variable Be stars in the LMC. We assume a combined foreground and intrinsic reddening of E(B-V) = 0.295. Error bars are based on a ±0.10 estimated error for B stars on or very close to the main bar. The observed position of (B-V) = 0 is shown by the broken vertical line. There is a mild correlation up to E(B-V) of ~ 0.3 but as the colour index increases the relation breaks down. Giant stars are again shown in black and main-sequence stars are shown in red.
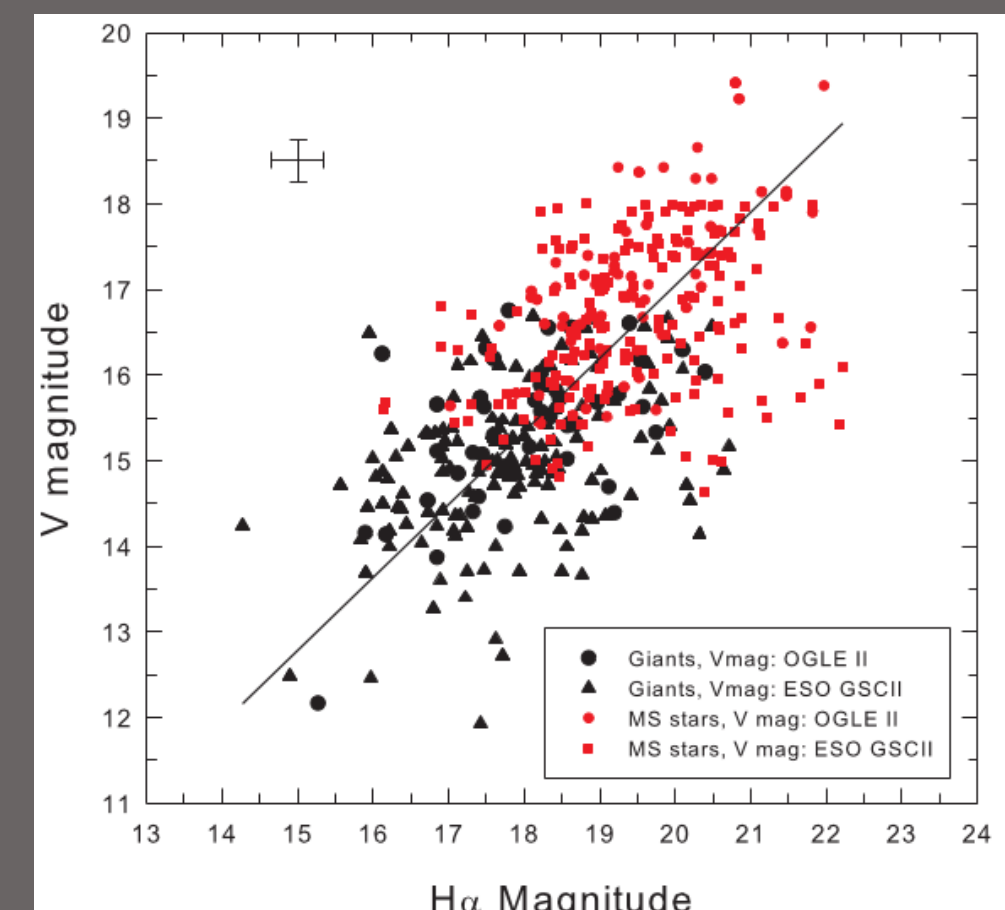
Figure 17. The luminosity of Hα emission from stars in the LMC is compared with their V magnitude. Giants and main-sequence stars are separated and assigned black and red colours respectively. A mild correlation can be seen down to the faint cut-off of V=18 for the ESO GSCII dataset. The linear line of regression indicates that Hα magnitudes are generally 2.76 magnitudes fainter than the visual magnitude for these stars. The correlation coefficient is 0.578 and the equation: $V_{mag} = 0.8507 × H\alpha$, may be used as a rough estimate. Maximum expected errors (shown) are based on previously published errors (for V) and measurement/calibration errors (for Hα).

Variability

The variable nature of Be and B[e] stars (Figure 18) is an important feature which relates to the physical stability of the star. As a phenomenon, it has been known for more than a century and may be due to a combination of physical properties, one or more of which may undergo a transition. Suggested mechanisms are mass loss through stellar winds, rapid rotation and/or non-radial pulsations. These mechanisms, individually or in combination, are usually proposed to explain disc formation and outbursts in Be stars.
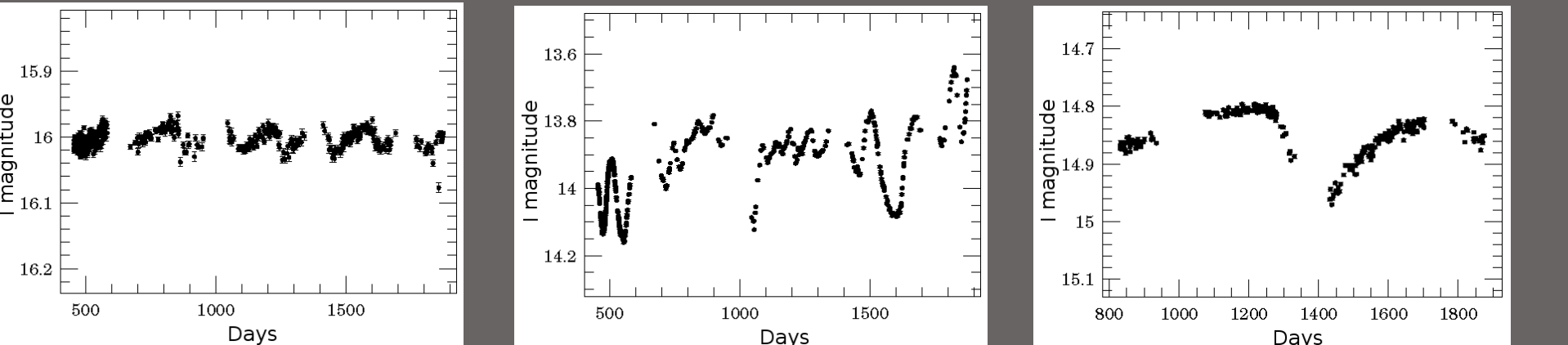

Figure 18. Three examples of the typical variability patterns found in LMC emission-line stars using OGLEII data. Shown are RPs1383, RPs870 and RPs1173.

References

Bohannan B.E., Epps H.W., 1974, A&AS, 18, 47
Bjorkman K. S., Miroshnichnichenko A.S., McDavid D., Pogrosheva T.M. 2002 ApJ, 573, 812
Dachs J., Hanuschik R.W., Kaiser D., Rohe D., 1986, AA., 159, 276
Gordon K.D., et al., 2003, ApJ., 594, 279
Grebel E.K., Chu Y., 2000, AJ, 199, 787
Hanuschik R.W., 1989, Ap&SS, 161, 61
Henize K.G., 1956, ApJS, 2, 315
Hummel W., et al. 1999 A&A 352, L31
Jaschek M., Jaschek C. 1967, ApJ., 150, 355

Keller S.C., Wood P.R., Bessell M.S., 1999, A&AS, 134, 489
Keller S.C., Bessell M.S., Da Costa G.S., 2000, AJ, 119, 1748
Olsen K.A.G., Kim S., Buss J.F., 2001 AJ, 121, 3075
Porter J.M., 1996, MNRAS, 280, 31
Reid W.A., Parker Q.A. 2006a, MNRAS, 365, 401
Reid W.A., Parker Q.A. 2006b, MNRAS., 373, 521
Reid W.A., Parker Q.A. 2010, (RPc) MNRAS., 405, 1349
Reid W.A., Parker Q.A. 2012 MNRAS 425, 355
Sabogal B.E., et al. 2005, MNRAS, 361, 1055
Struve O., 1931, ApJ, 73, 94
Underhill A., Doazan V., 1982, 'B STARS with and without emission' NASA SP-456
Wisniewski J.P., Bjorkman K.S., 2006 ApJ, 652, 458